Geophysical Research Letters

RESEARCH LETTER
10.1029/2021GL093905

Key Points:

- Global-scale Observations of Limb and Disk (GOLD) thermospheric temperature increases globally in response to geomagnetic activity
- The increase in temperature is proportional to the strength of the activity and is greater at higher latitudes
- Temperature enhancement during active geomagnetic events is greater in the morning than that in the afternoon

Correspondence to:
F. I. Laskar,
Fazlul.Laskar@colorado.edu

Citation:
Laskar, F. I., Eastes, R. W., Codrescu, M. V., Evans, J. S., Burns, A. G., Wang, W., et al. (2021). Response of GOLD retrieved thermospheric temperatures to geomagnetic activities of varying magnitudes. *Geophysical Research Letters*, *48*, e2021GL093905. https://doi.org/10.1029/2021GL093905

Received 16 APR 2021
Accepted 15 JUL 2021

Response of GOLD Retrieved Thermospheric Temperatures to Geomagnetic Activities of Varying Magnitudes

F. I. Laskar[1], R. W. Eastes[1], M. V. Codrescu[2], J. S. Evans[3], A. G. Burns[4], W. Wang[4], W. E. McClintock[1], S. Aryal[1], and X. Cai[4]

[1]Laboratory for Atmospheric and Space Physics, University of Colorado, Boulder, CO, USA, [2]Space Weather Prediction Center, NOAA, Boulder, CO, USA, [3]Computational Physics, Inc., Springfield, VA, USA, [4]High Altitude Observatory, National Center for Atmospheric Research, Boulder, CO, USA

Abstract Global-scale Observations of Limb and Disk (GOLD) disk measurements of far ultraviolet molecular nitrogen band emissions are used to retrieve temperatures (T_{disk}), which are representative of lower thermospheric altitudes. The present investigation studies the response of lower thermospheric temperatures to geomagnetic activities of varying magnitudes. In this study, it has been observed that T_{disk} increases over all latitudes in response to enhanced geomagnetic activity. The increase in temperature is proportional to the strength of the geomagnetic activity and is greater at higher latitudes. Temperature enhancements vary from 10s to 100s of Kelvins from low- to mid-latitudes. Local time behavior shows that pre-noon enhancements in temperatures, during relatively stronger geomagnetic activities, are greater compared to afternoon, which may be caused by the combined action of daytime dynamics and geomagnetic forcing. This study, thus, demonstrates the utility of GOLD T_{disk} when investigating the effects of dynamical and external forcings in the thermosphere.

Plain Language Summary The thermosphere ionosphere system is influenced by waves from the lower atmosphere and solar and geomagnetic forcing from above. For such a coupled system it is important to decipher the relative influence of the two regimes of forcings. The recently launched Global-scale Observations of Limb and Disk (GOLD) mission provides daytime thermospheric temperatures with unprecedented local time and spatial coverage. The thermospheric temperature over the Earth's disk visible from geostationary orbit is a first of its kind of measurement, which enables us to investigate the local time behavior over wide latitudinal coverage from 69°S to 69°N. We find that, during active geomagnetic conditions, the thermospheric temperature is enhanced across the whole visible hemisphere, with the largest temperature enhancements at higher mid-latitudes. The local time behavior shows that the pre-noon enhancement in temperature is greater compared to the afternoon, which demonstrates, for the first time, a systematic local time varying response of thermosphere to geomagnetic forcing.

1. Introduction

Temperature variability of the daytime thermosphere of the Earth is controlled mainly by solar radiation. It is also influenced by wave forcing from the lower atmosphere and geomagnetic forcing from above. During geomagnetic storms energetic particle precipitation at high-latitudes induces, among other effects, ionospheric current systems, Joule heating, and large-scale circulation changes (Burns & Killeen, 1992; Deng et al., 1995; Forbes et al., 1996; Killeen et al., 1997; Mayr et al., 1978; Prölss, 1980; Rishbeth & Garriott, 1969). The impact of the currents generated by the movement of the energetic particles and the ionization they produce is instantaneous and they can indirectly alter the low-latitude ionosphere (Tsurutani et al., 2008). The most important heating term is the Joule heating (per particle), and the ion-neutral momentum coupling induced by circulation changes gives rise to delayed impacts at different latitudes and altitudes in the thermosphere (Burns et al., 1995; Mayr et al., 1978; Prölss, 1980).

Depending on the strength of a geomagnetic storm, the thermospheric circulation can reverse from the usual poleward daytime circulation. Storm induced circulation changes can also give rise to relative adiabatic cooling or heating depending on the relative changes in the divergence and convergence of the horizontal winds. Radiative cooling by infrared emissions from nitric oxide (NO) and carbon dioxide (CO_2) is the

mechanism through which energy is dissipated in the lower thermosphere (Killeen et al., 1997; Mikhailov & Perrone, 2020). In short, a geomagnetic storm can alter the whole thermosphere-ionosphere (TI) system enormously, so synoptic observations of local time variability of the thermosphere during storm events are important for a complete understanding of space weather.

The neutral atmosphere at TI altitudes (about 100 km and up) is primarily investigated using in-situ (e.g., Forbes et al., 1996; H. Liu & Lühr, 2005; Spencer et al., 1981) and optical remote sensing techniques (Aksnes et al., 2006; Meier et al., 2015; Pallamraju et al., 2004, 2013; Pant & Sridharan, 1998). The temperature of the thermosphere can be retrieved from spectral broadening characteristics of atomic lines (Biondi & Meriwether, 1985; Chakrabarty et al., 2002; Fagundes et al., 1996; Pant & Sridharan, 1998) or molecular bands (Aksnes et al., 2006; Evans et al., 2018; Meier et al., 2015; Zhang et al., 2019). Ground based observations of the thermosphere have good local time coverage, at a cadence of minutes to hours for over at least 10 h per day, but they are mostly limited to the night-time sector and are available from limited ground stations (Biondi & Meriwether, 1985; Chakrabarty et al., 2002; Fagundes et al., 1996; Pant & Sridharan, 2001). Satellite based remote-sensing observations on the other hand have poor local time coverage and are mostly from limb viewing geometry (Aksnes et al., 2006; Meier et al., 2015). In-situ temperature measurements are also very limited, for example, those from Dynamic Explorer 2 (DE-2) mission (Spencer et al., 1981) or those retrieved from satellite drag (e.g., Mehta et al., 2017, and references therein). As most of the earlier satellite missions measuring thermospheric parameters were in quasi-sun synchronous orbits, they lack local time coverage. However, a constellation of quasi-sun-synchronous low earth orbits or very low inclination orbits can provide good local time coverage, but such configurations have not been used so far for thermospheric measurements. Thus, the earlier studies provided mostly a seasonally averaged or near-single local time behavior of the thermospheric temperature variability during geomagnetic activities. Therefore, the local time variations of the geomagnetic storm effects on thermospheric temperatures with global coverage have been limited mainly to model simulations (Burns et al., 1995). For a wide spatial and local time coverage one would require ground based stations covering the globe, or a constellation of sun-synchronous satellites in low-earth-orbit, or measurements from the geo-stationary orbit. The Global-scale Observations of the Limb and Disk (GOLD) mission, launched on January 14, 2018, is in geostationary orbit and provides Far-Ultraviolet (FUV) emission measurements, which can be used to retrieve thermospheric neutral temperatures (Eastes et al., 2020). Though GOLD disk measurements are limited over a fixed hemisphere, they have very good coverage in latitude (69°S to 69°N), longitude (25°E to 120°W; covering America and parts of Europe and Africa), and local time (a minimum of 6–18 h near nadir longitude, which extends to even more local times depending on location).

Evidence of geomagnetic storm related changes in thermospheric temperatures, densities, and winds are ample in the literature (Aksnes et al., 2007; Astafyeva et al., 2020; Bagiya et al., 2014; Burns & Killeen, 1992; Burns et al., 1995; Crowley et al., 2006; Karan & Pallamraju, 2018; Mandal & Pallamraju, 2020; Mayr et al., 1978; Pallamraju et al., 2004; Pant & Sridharan, 2001; Strickland et al., 1999; Zhang et al., 2019). Due to particle precipitation, the temperatures at high-latitude are increased and the resulting circulation changes alter the whole thermospheric temperature (Burns & Killeen, 1992; Burns et al., 1995; Fuller-Rowell et al., 1994) with some delayed response at different altitudes and latitudes (Burns et al., 1995; Li et al., 2018; X. Liu et al., 2018). Some recent investigations using GOLD O/N_2 (ratio of atomic oxygen and molecular nitrogen column densities) (Cai, Burns, Wang, Qian, Pedatella, et al., 2021; Cai, Burns, Wang, Qian, Solomon, et al., 2021), oxygen-I (OI) 135.6 nm emission intensities (Gan et al., 2020), and limb temperature (Evans et al., 2020) data showed that even minor to moderate geomagnetic activities can impact the TI system significantly. But the majority of the earlier investigations of daytime thermospheric variability lack the local time and spatial coverage provided by the GOLD mission from geosynchronous orbit. The current study aims to use GOLD neutral disk temperature (T_{disk}) data to investigate synoptic and local time behavior of the thermospheric temperature during periods of enhanced geomagnetic activity of varying magnitudes.

2. Data and Methods

The primary data set used in this investigation is the GOLD retrieved neutral disk temperatures, T_{disk}. Solar and geomagnetic indices are also used. GOLD observes the Earth's thermosphere in the FUV for over 18.5 h each day, from 0610 to 0040 UT of the next day (Eastes et al., 2019, 2020; Laskar et al., 2020; McClintock

et al., 2020). The day-disk measurements cover about 0610 UT to 2300 UT, of which the majority of the disk falls in the day-light sector for about 9 h. GOLD daytime disk scans of the N_2 Lyman-Birge-Hopfield (LBH) bands are used to retrieve the T_{disk} data. As the GOLD N_2 LBH emission measurements are column integrated quantities, the retrieved T_{disk} products are a representative of the corresponding N_2 LBH layer. The peak altitude of the layer has a range of 150–220 km which varies with solar zenith angle (SZA) and emission angle. But the peak altitudes remain below 200 km for SZA and emission angles less than 70° (Evans et al., 2018; Laskar et al., 2021). GOLD scans each full disk in about 30 min. The retrieval algorithm is an improvement of the code that was used previously to derive temperature from limb measurements of N_2 LBH intensity from the High-resolution Ionospheric and Thermospheric Spectrograph (HITS) instrument (Aksnes et al., 2006; Krywonos et al., 2012). GOLD measurements have a higher spectral resolution that includes N_2 LBH band emissions within 132–162 nm range. Effective neutral temperatures are retrieved by fitting the observed rotational structure of the N_2 LBH bands using an optimal estimation routine (Evans et al., 2018; Lumpe et al., 2002; Rodgers, 2000). Five parameters are retrieved from each measured spectrum: rotational temperature (K), wavelength shift and dispersion (nm), background (counts/bin), and a forward model scale factor. The current investigation used Level 2 (L2) T_{disk} version 3 (V03) data that are retrieved from 2×2 binned level-1C N_2 LBH spectra, which are available at the GOLD web-page, https://gold.cs.ucf.edu/. The 2×2 binned data have a spatial resolution of 250-km × 250-km near nadir. Typical random errors in the 2×2 binned T_{disk} data varies with signal-to-noise ratio (SNR) of the N_2 LBH emission and it ranges from 20 K (for high SNR) to 600 K (for low SNR). The arithmetic mean of the errors over the disk and for all local times is about 45 K. An earlier version (V02) of T_{disk} data were retrieved from unbinned L1C data. The random error in those data were more than seven times higher than the current version, so we are using the V03 2×2 data for the current investigation.

3. Results

Sub-satellite local time (Sub-Sat. LT) versus day-to-day variation of GOLD T_{disk} (from here on temperature or in short T) for about 2.5 years (October 14, 2018–March 15, 2021) of observations with ap index and solar F10.7 flux are shown in Figure 1a. These are averaged between 21°N to 53°N and 43°W to 54°W from the disk observations. This spatial bin is chosen arbitrarily and any other spatial combination also shows similar behavior. But selection of a very narrow bin results in a noisy signal. The average random uncertainty, which varies with LBH emission SNR, within the above chosen spatial bin is about 12 K. Notable features in this figure are: (a) the temperature is highest near 13–14 LT and afternoon is warmer than morning, and (b) the temperature increases over all local times in response to an increase in ap index or F10.7 flux. Figure 1b shows temperature deviations (ΔT) from a baseline local time behavior. The baseline levels are calculated using all the quiet days (with ap < 6 nT) that are within a 30-day running window of observation. Since the mean of the ap values during these 2.5 years of observations is 6.1 ± 4.8 nT, we use ap < 6 nT to define geomagnetically quiet times. We choose a 30-day window so that the seasonal changes are also removed once we subtract the 30-day mean. A shorter window will have fewer days with ap < 6 nT and also we do not want to remove variations shorter than 30 days, where most of the dominant geomagnetic variations fall.

Though the solar flux has not exceeded 120 sfu (1 sfu = 10^{-22} $Wm^{-2}Hz^{-1}$) during the period covered in this study, the temperatures show some increase with the slight enhancement in F10.7 cm flux during the last quarter of 2020, where it was above 110 sfu for a couple of days. This temperature increase with F10.7 cm flux is above the random uncertainty, which is about 12 K. A notable feature of ΔT, as shown in Figure 1b, is that it increases with increasing ap index. Thus, observations in Figure 1 demonstrate that the GOLD temperature responds to both solar flux and geomagnetic activity. These findings are consistent with the response observed in GOLD exospheric temperatures due to minor geomagnetic activity reported by Evans et al. (2020). In addition to variations that are related to geomagnetic activity, annual variations can also be seen, for example, the winter (summer) morning temperatures are relatively colder (warmer) in Figure 1a. These annual variations are very interesting and will be addressed in a separate investigation. There is a gap of about 10 days of data during April 16–26, 2019, where the GOLD channel-A detector gain was low, which needed a grating yaw maneuver to overcome this. The data during this interval are available but should be interpreted with caution. Thus, they are not used in the present investigation. Due to this data gap the

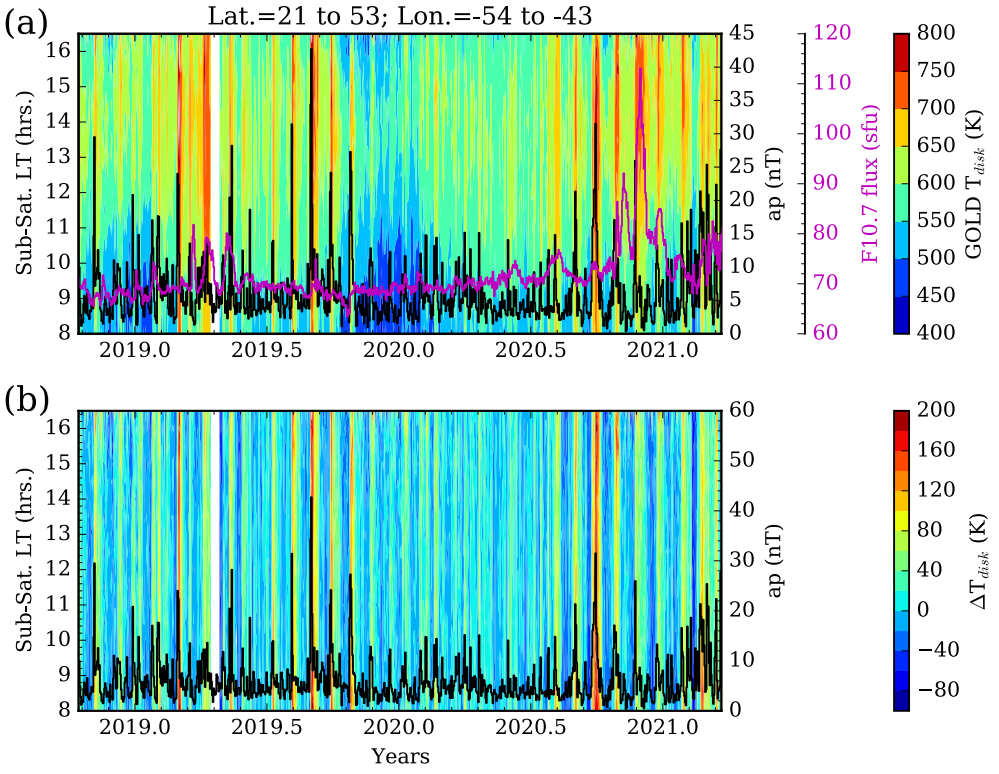

Figure 1. Sub-satellite local time and day-to-day variation of Global-scale Observations of Limb and Disk (GOLD) temperature for about 2.5 years of observations along with ap index and solar F10.7 cm flux are shown in (a). ΔT and ap index variation are shown in (b). Notable feature is the enhancement in T and ΔT as the ap index increase.

effective number of days having ap < 6 nT will be smaller, but there are sufficient number of days with ap < 6 nT within these 30 days windows to calculate the quiet-time background.

To quantify the relationship between ap and ΔT, a scatter plot and a linear regression analysis are shown in Figure 2a. The scatter plot and the correlation analysis are done with the averaged ΔT values between 21°N to 53°N and 43°W to 54°W and 10–14 h local time for all the days. The choice of local time range does not change the results significantly, but only impacts the random uncertainty (not presented here) but the choice of latitude range impacts the ΔT. Each point in the scatter plot represents a day averaged within the above local-time and spatial bin. A correlation coefficient of ~ 0.64 is observed between ap and ΔT, which indicates that they are positively, though weakly, correlated. The not so strong positive correlation between ap and ΔT can be due to other sources of temperature variability, for example, lower atmospheric waves (Laskar et al., 2013, 2014) and non-linear response of temperature to geomagnetic-forcing (Connor et al., 2016), and solar flux variability. To further quantify their variabilities, Lomb-Scargle periodograms (Horne & Baliunas, 1986) of ap, F10.7, and T_{disk} are shown in Figure 2b. Almost all the dominant periodicities that are seen in ap, such as, 6, 7, 9, 13–15, and 23–30 days can also be seen in T_{disk}. These results demonstrate that the thermospheric temperature responds positively to geomagnetic activity. The F10.7 cm flux show some dominant periodicities around 27-day, the solar rotational period, which can also be seen in T_{disk} and ap periodicities.

As GOLD provides good latitude coverage from 69°S to 69°N, a latitudinal variation of correlation coefficients between ap and ΔT is shown in Figure 3a for two ap ranges, 8–14 nT and ≥ 14 nT. The local time and longitude ranges are the same as that of Figure 2. The ap values below 8 nT are not used in this analysis as the geomagnetic activities during such ap magnitudes are not expected to influence the temperature as the base-level ap value is about 6 nT. The number of days with 8 nT ≤ ap < 14 nT and ap ≥ 14 are 111 and 52, respectively. Some of the active events lasted for more than a day, so the number of individual active periods with 8 nT ≤ ap < 14 nT and ap > 14 nT were at least 50 and 27, respectively. The latitudinal variation of ΔT for

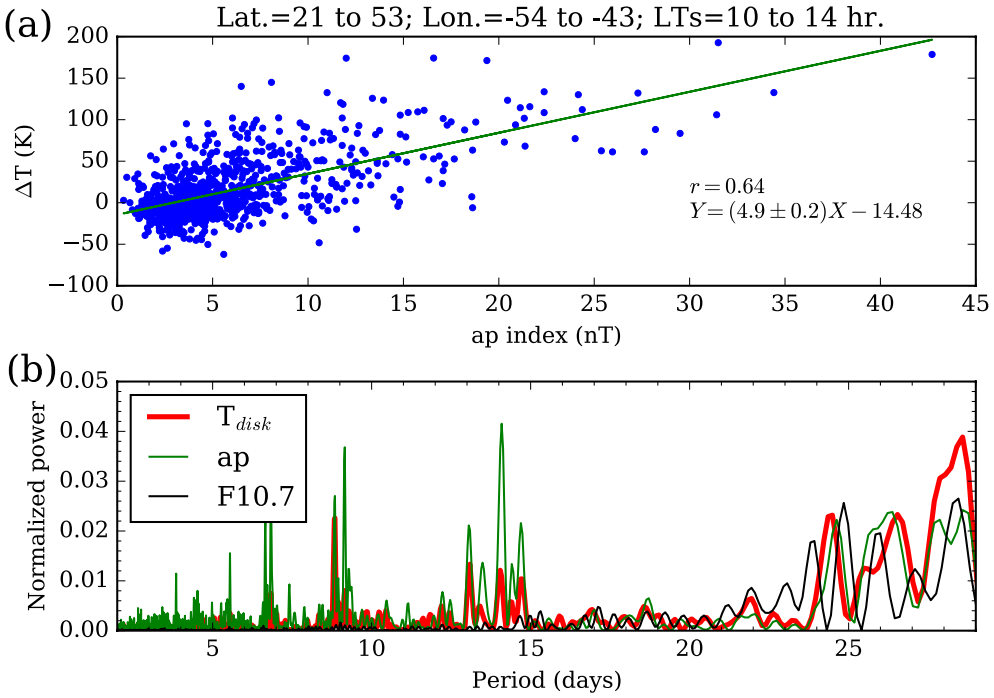

Figure 2. Scatter plot and linear regression with Pearson correlation coefficient between ΔT and ap are shown in (a). Lomb-Scargle periodograms of ap, F10.7 flux, and ΔT are shown in (b). A positive correlation of about 0.64 is observed at latitudes between 21-53°N. Periodogram analysis shows that most of the dominant peaks in ΔT can also be seen in ap.

the two geomagnetic activity ranges is shown in Figure 3b. The temperature retrieval algorithm is not optimized to take into account the changes in LBH emissions due to energetic particle precipitation, so latitudes higher than 60° are not considered in this analysis. Note that the correlation coefficients are positive at all latitudes and are higher for stronger geomagnetic events. Also, the temperature enhancements are always positive and are greater at higher mid-latitudes. The greater ΔT enhancements at higher mid-latitudes are in accordance with the fact that most of the energy deposition of the storm time particle precipitation occurs at high-latitudes. As the northern geomagnetic pole, for the current longitude sector, is closer to geographic equator the temperature enhancements are greater for the northern latitudes compared to southern hemisphere higher latitudes. It also demonstrates that the temperature enhancements occur over all latitudes. The percentage increase in ΔT varies from 10% to 20% for the stronger events. These percentages are for an average of all the 27 individual events having ap ≥ 14 nT. However, the strongest event on August 31 to September 1, 2019 with a daily average ap of 43 nT showed about 25%–35% enhancement in temperature at low- to mid-latitudes. As the ΔT values are calculated using a reference quiet-day that is, obtained from a 30-day running mean around the active day, they should be independent of any artifact that may arise from SZA and emission angle dependence of T_{disk} (Evans et al., 2018). The higher temperatures at mid-latitudes as reported in the current work can induce thermospheric pole to equatorward circulation that transports oxygen rich air toward low-latitudes (Mayr et al., 1978), giving rise to enhanced OI 135.6-nm emission intensities at low-latitudes and decreased intensities at mid- and high-latitudes (e.g., Gan et al., 2020).

A unique feature of the GOLD mission is that it provides an unprecedented local time coverage, in addition to a wide spatial coverage. To investigate the local time variabilities, T and ΔT variation at northern mid-latitudes (32°N to 53°N) for the days with ap > 20 nT are shown in Figure 4. Note that the number of individual active events with ap > 20 nT was 16 in the 2.5 years period. Of the 16 active events, many of them lasted for several days. For this analysis only the first day of the active events is considered when comparing them with a pre-active quiet day. For a particular event, the pre-active quiet day is selected from five consecutive days just prior to the first active day. The day with minimum ap value among these 5 days is regarded as the quiet day. For most of the events the pre-active quiet day falls 2–3 days before the first active day. As

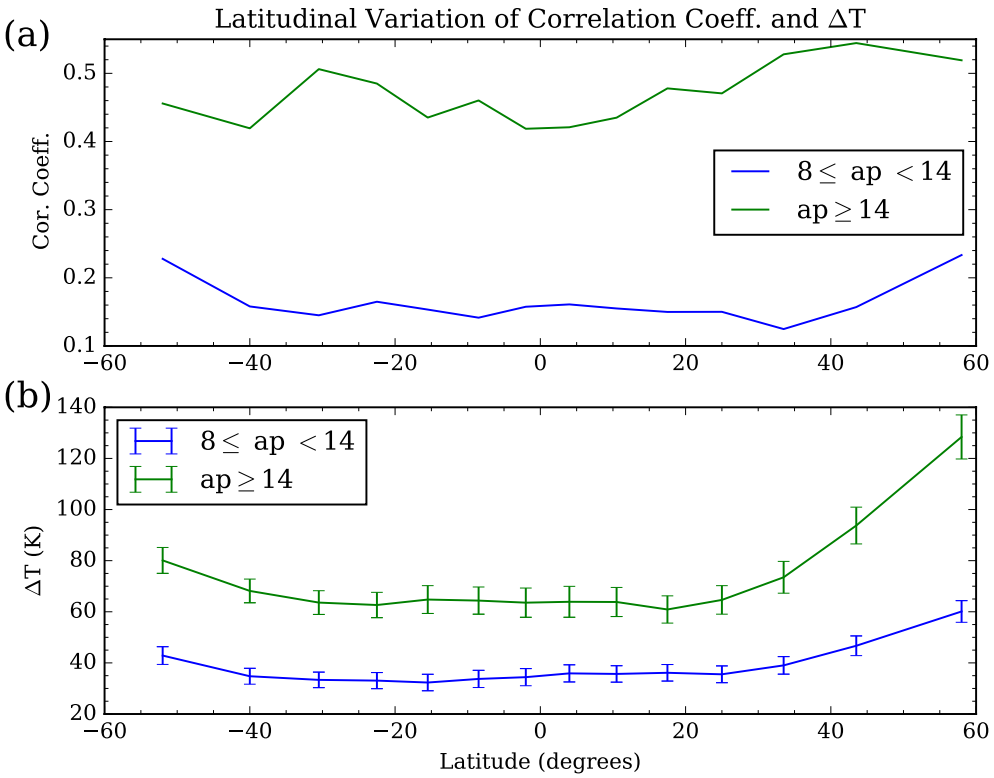

Figure 3. Latitudinal variation of correlation coefficients between ap and ΔT are shown in (a) for two ap limits, $8 \leq ap < 14$ nT and $ap \geq 14$ nT. Latitudinal variation of ΔT is shown in (b) for the two activity ranges. Correlation coefficients are positive at all latitudes and the temperature enhancements are greater at higher mid-latitudes.

there are 16 individual active events having ap > 20 nT, the calculations in Figure 4 used 16 active and 16 quiet days. Average ap indices for the 16 quiet and 16 active days were 2.9 and 25.4 nT, respectively. Also, the average F10.7 cm flux for the quiet and active days were 72.1 and 73.0 sfu, that is, they are nearly the same. It can be seen in Figure 4 that there is more than 90 K difference between active and quiet times at all local times, which cannot be attributed to the 1 sfu increase in F10.7 cm flux. Note that the morning time (8–12 LT) temperature deviations are 23.5 ± 2.5 K larger compared to afternoon time (12.5–16.5 LT). Such morning and afternoon temperature differences are seen primarily at mid-latitudes and the differences are very small or absent at low-latitudes (not shown here). This morning and afternoon difference is higher for the stronger events and they are nearly absent, even at mid-latitudes, for events having ap index less than 20 nT. This is the reason why ap = 20 nT is chosen as a lower limit for the morning and afternoon difference investigation. Also, the latitude range is changed to mid-latitude only as these differences are prominent at mid-latitudes (Burns et al., 1995) and are very small or absent at low-latitudes for majority of the events. Note that the strongest geomagnetic event during the current observation period is of moderate strength that occurred during August 31 to September 1, 2019. In the future, when we expect a greater number of moderate and severe geomagnetic storms, a quantitative investigation of the relationship between strength of geomagnetic activity and corresponding morning to afternoon temperature difference at low and mid-latitudes could be performed.

4. Discussion

Heating due to solar Extreme-Ultra-Violet (EUV) absorption and cooling due to downward heat transport are the primary source and sink of energy in the daytime thermosphere. The diurnal tidal circulation in the thermosphere is mainly driven by in-situ differential heating due to solar EUV. As a result of this circulation there occur regions of convergence and divergence that produce vertical motions (Laskar et al., 2017), which are upward in the daytime and are downward in the majority of the night-sector at low- and mid-latitudes

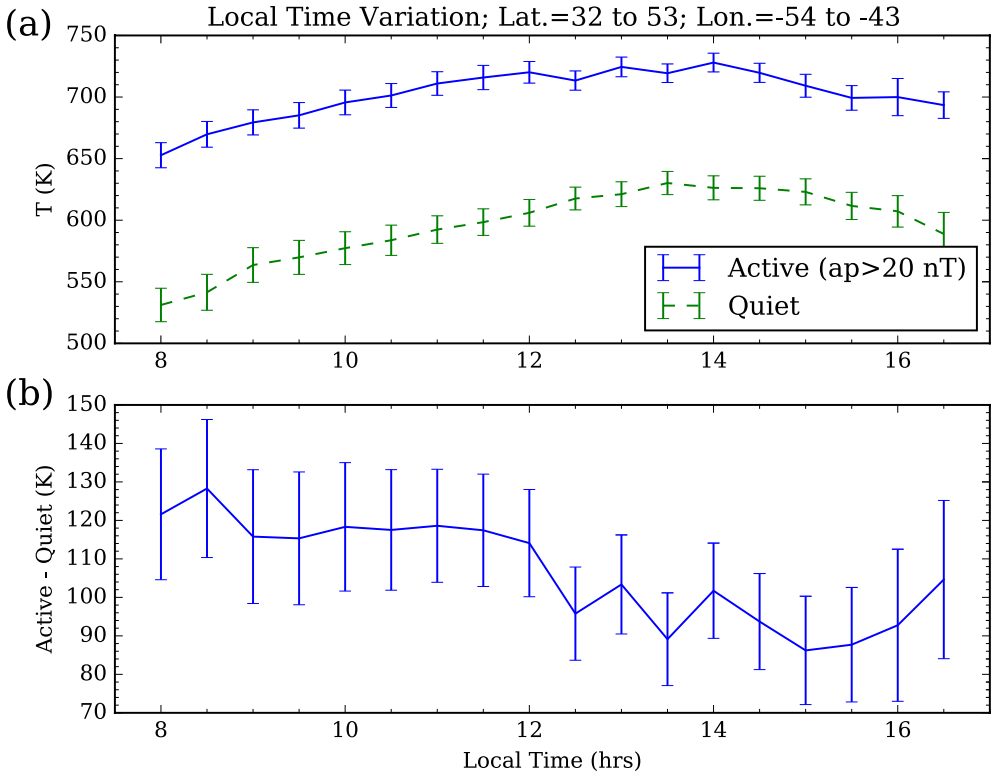

Figure 4. Mean *T* variations at northern mid-latitudes for all the days with ap > 20 nT and average of their corresponding pre-storm (Quiet) days are shown in (a). The difference between active and quiet days are shown in (b). Morning time (8–12 LT) differences are greater compared to afternoon time (after 12 LT).

(Burns et al., 1995; Mayr et al., 1978). From numerical model simulations, Burns et al. (1995) showed that under quiet geomagnetic conditions the usual vertical winds during late-night to late-morning are downward and that they are upward in the afternoon and late-evening sector. During geomagnetically active events the usual thermospheric equator to pole circulation gets disturbed due to high-latitude energy deposition. Under such altered circulation, the morning time vertical winds at low- and mid-latitudes become increasingly downward due to pole to equator circulation thus creating greater compressional heating compared to quiet time. Whereas, in the afternoon and evening sectors, the storm time circulation makes the vertical winds weaker, resulting in less expansion of the thermosphere and thus less cooling. Due to this change in circulation, the storm-time temperatures at low- and mid-latitudes are higher than quiet time. This mechanism suggests that the pre-noon sector enhancement in thermospheric temperature would be greater than in the afternoon. Figure 8 of Burns et al. (1995) shows a numerical simulation result that provides a more detailed explanation of this mechanism. The DE-2 data used in Burns et al. (1995) were extremely limited and thus could not demonstrate the effect unambiguously. The numerical model simulation results of Burns et al. (1995) provide a plausible explanation of the GOLD observed morning and afternoon temperature difference as shown in Figure 4. Therefore, the GOLD results presented in Figure 4 provide a first experimental demonstration of this effect during geomagnetically active conditions. This has been possible due to the unprecedented local-time and latitude coverage of the GOLD mission. Further studies are warranted on the possible association of the morning and afternoon difference to the day-night difference of the magnetospheric energy input to the high-latitude thermosphere. In the future, a more detailed investigation of GOLD observations during stronger geomagnetic storms could be performed to quantify the temporal relationship between different phases of the storms and ΔT.

5. Conclusions

An investigation of the response of thermospheric temperatures to geomagnetically active events of varying magnitudes is carried out using recently available GOLD L2 T_{disk} data. The salient results of this investigation are:

1. Global-scale Observations of Limb and Disk (GOLD) T_{disk} measurements respond to geomagnetic activity of varying magnitudes and the response is proportional to the strength of the activity.
2. T_{disk} responds to even minor geomagnetic activity with an ap values less than 14 nT.
3. The temperature enhancement increases with increasing latitude and they are observed to vary from 10% to 35% for weak to moderate events.
4. The pre-noon increase in temperature is about 23 K larger than the afternoon one for the active events with ap > 20 nT. This demonstrates that the usual daytime circulation and storm altered circulation work in phase in the pre-noon sector. This also provides a first experimental demonstration of earlier numerical model simulation studies.

These observational results demonstrate, for the first time, a systematic local time varying response of thermosphere to geomagnetic forcing. This investigation also indicates that the GOLD T_{disk} data can be used for space weather and operational use. Possible future investigations could be done on the latitude, longitude, and local time dependence of the effect of geomagnetic storms on thermospheric variability and their spatio-temporal relationship with different phases of the storms.

Data Availability Statement

The Level 2 data used in this study are available at the GOLD Science Data Center (https://gold.cs.ucf.edu/search/) and at NASA's Space Physics Data Facility (https://spdf.gsfc.nasa.gov/pub/data/gold/level2/tdisk/). The ap index and F10.7 flux data are obtained from NASA omniweb (https://omniweb.gsfc.nasa.gov/).

Acknowledgments
This research study was supported by NASA Contract 80GSFC18C0061 to the University of Colorado, Boulder. This material is also based upon work supported by the National Center for Atmospheric Research (NCAR), which is a major facility sponsored by the National Science Foundation under Cooperative Agreement No. 1852977. This work was also supported in part by NASA HSR grants 80NSSC19K0835 and NNX17AI42G.

References

Aksnes, A., Eastes, R., Budzien, S., & Dymond, K. (2006). Neutral temperatures in the lower thermosphere from N_2 Lyman-Birge-Hopfield (LBH) band profiles. *Geophysical Research Letters*, *33*(15). https://doi.org/10.1029/2006gl026255

Aksnes, A., Eastes, R., Budzien, S., & Dymond, K. (2007). Dependence of neutral temperatures in the lower thermosphere on geomagnetic activity. *Journal of Geophysical Research*, *112*(A6). https://doi.org/10.1029/2006ja012214

Astafyeva, E., Bagiya, M. S., Förster, M., & Nishitani, N. (2020). Unprecedented hemispheric asymmetries during a surprise ionospheric storm: A game of drivers. *Journal of Geophysical Research: Space Physics*, *125*(3). https://doi.org/10.1029/2019ja027261

Bagiya, M. S., Hazarika, R., Laskar, F. I., Sunda, S., Gurubaran, S., Chakrabarty, D., et al. (2014). Effects of prolonged southward interplanetary magnetic field on low-latitude ionospheric electron density. *Journal of Geophysical Research: Space Physics*, *119*(7), 5764–5776. https://doi.org/10.1002/2014ja020156

Biondi, M. A., & Meriwether, J. W. (1985). Measured response of the equatorial thermospheric temperature to geomagnetic activity and solar flux changes. *Geophysical Research Letters*, *12*(5), 267–270. https://doi.org/10.1029/gl012i005p00267

Burns, A. G., & Killeen, T. L. (1992). The equatorial neutral thermospheric response to geomagnetic. *Geophysical Research Letters*, *19*(10), 977–980. https://doi.org/10.1029/92gl00522

Burns, A. G., Killeen, T. L., Deng, W., Carignan, G. R., & Roble, R. G. (1995). Geomagnetic storm effects in the low- to middle-latitude upper thermosphere. *Journal of Geophysical Research*, *100*(A8), 14673. https://doi.org/10.1029/94ja03232

Cai, X., Burns, A. G., Wang, W., Qian, L., Pedatella, N., Coster, A., et al. (2021). Variations in thermosphere composition and ionosphere total electron content under "geomagnetically quiet" conditions at solar-minimum. *Geophysical Research Letters*, *48*(11). https://doi.org/10.1029/2021gl093300

Cai, X., Burns, A. G., Wang, W., Qian, L., Solomon, S. C., Eastes, R. W., et al. (2021). Investigation of a neutral "tongue" observed by GOLD during the geomagnetic storm on May 11, 2019. *Journal of Geophysical Research: Space Physics*, *126*(6). https://doi.org/10.1029/2020ja028817

Chakrabarty, D., Pant, T. K., Sekar, R., Taori, A., Modi, N. K., & Narayanan, R. (2002). Thermospheric temperature and magnetic field measurements from Mt Abu during a geomagnetically disturbed period—A case study. *Current Science*, *83*(2), 167–170. Retrieved from www.jstor.org/stable/24106222

Connor, H. K., Zesta, E., Fedrizzi, M., Shi, Y., Raeder, J., Codrescu, M. V., & Fuller-Rowell, T. J. (2016). Modeling the ionosphere-thermosphere response to a geomagnetic storm using physics-based magnetospheric energy input: Open GGCM-CTIM results. *Journal of Space Weather and Space Climate*, *6*, A25. https://doi.org/10.1051/swsc/2016019

Crowley, G., Hackert, C. L., Meier, R. R., Strickland, D. J., Paxton, L. J., Pi, X., et al. (2006). Global thermosphere-ionosphere response to onset of 20 November 2003 magnetic storm. *Journal of Geophysical Research*, *111*(A10). https://doi.org/10.1029/2005ja011518

Deng, W., Killeen, T. L., Burns, A. G., Johnson, R. M., Emery, B. A., Roble, R. G., et al. (1995). One-dimensional hybrid satellite track model for the dynamics explorer 2 (DE 2) satellite. *Journal of Geophysical Research*, *100*(A2), 1611. https://doi.org/10.1029/94ja02075

Eastes, R. W., McClintock, W. E., Burns, A. G., Anderson, D. N., Andersson, L., Aryal, S., et al. (2020). Initial observations by the GOLD mission. *Journal of Geophysical Research: Space Physics*, *125*(7). https://doi.org/10.1029/2020ja027823

Eastes, R. W., Solomon, S. C., Daniell, R. E., Anderson, D. N., Burns, A. G., England, S. L., et al. (2019). Global-scale observations of the equatorial ionization anomaly. *Geophysical Research Letters*, *46*(16), 9318–9326. https://doi.org/10.1029/2019gl084199

Evans, J. S., Eastes, R., Lumpe, J. D., Correira, J., Burns, A. G., McClintock, B., et al. (2018). Global-scale Observations of the Limb and Disk (GOLD): Overview of Daytime Neutral Temperature Science Data Product. *Agu Fall Meeting Abstracts* (Vol. 2018, p. SA21A3172).

Evans, J. S., Lumpe, J. D., Correira, J., Veibell, V., Kyrwonos, A., McClintock, W. E., et al. (2020). Neutral exospheric temperatures from the GOLD mission. *Journal of Geophysical Research: Space Physics*, *125*(9). https://doi.org/10.1029/2020ja027814

Fagundes, P., Sahai, Y., Takahashi, H., Gobbi, D., & Bittencourt, J. (1996). Thermospheric and mesospheric temperatures during geomagnetic storms at 23 °S. *Journal of Atmospheric and Terrestrial Physics*, *58*(16), 1963–1972. https://doi.org/10.1016/0021-9169(96)00001-3

Forbes, J. M., Gonzalez, R., Marcos, F. A., Revelle, D., & Parish, H. (1996). Magnetic storm response of lower thermosphere density. *Journal of Geophysical Research*, *101*(A2), 2313–2319. https://doi.org/10.1029/95ja02721

Fuller-Rowell, T. J., Codrescu, M. V., Moffett, R. J., & Quegan, S. (1994). Response of the thermosphere and ionosphere to geomagnetic storms. *Journal of Geophysical Research*, *99*(A3), 3893. https://doi.org/10.1029/93ja02015

Gan, Q., Eastes, R. W., Burns, A. G., Wang, W., Qian, L., Solomon, S. C., et al. (2020). First synoptic observations of geomagnetic storm effects on the global-scale OI 135.6-nm dayglow in the thermosphere by the GOLD mission. *Geophysical Research Letters*, *47*(3). https://doi.org/10.1029/2019gl085400

Horne, J. H., & Baliunas, S. L. (1986). A prescription for period analysis of unevenly sampled time series. *The Astrophysical Journal*, *302*, 757. https://doi.org/10.1086/164037

Karan, D. K., & Pallamraju, D. (2018). Effect of geomagnetic storms on the daytime low-latitude thermospheric wave dynamics. *Journal of Atmospheric and Solar-Terrestrial Physics*, *170*, 35–47. https://doi.org/10.1016/j.jastp.2018.02.003

Killeen, T., Burns, A., Azeem, I., Cochran, S., & Roble, R. (1997). A theoretical analysis of the energy budget in the lower thermosphere. *Journal of Atmospheric and Solar-Terrestrial Physics*, *59*(6), 675–689. https://doi.org/10.1016/s1364-6826(96)00114-9

Krywonos, A., Murray, D. J., Eastes, R. W., Aksnes, A., Budzien, S. A., & Daniell, R. E. (2012). Remote sensing of neutral temperatures in the Earth's thermosphere using the Lyman-Birge-Hopfield bands of N_2: Comparisons with satellite drag data. *Journal of Geophysical Research*, *117*(A9). https://doi.org/10.1029/2011ja017226

Laskar, F. I., Chau, J. L., St-Maurice, J. P., Stober, G., Hall, C. M., Tsutsumi, M., et al. (2017). Experimental evidence of arctic summer mesospheric upwelling and its connection to cold summer mesopause. *Geophysical Research Letters*, *44*(18), 9151–9158. https://doi.org/10.1002/2017gl074759

Laskar, F. I., Eastes, R. W., Martinis, C. R., Daniell, R. E., Pedatella, N. M., Burns, A. G., et al. (2020). Early morning equatorial ionization anomaly from GOLD observations. *Journal of Geophysical Research: Space Physics*, *125*(7). https://doi.org/10.1029/2019ja027487

Laskar, F. I., Pallamraju, D., & Veenadhari, B. (2014). Vertical coupling of atmospheres: Dependence on strength of sudden stratospheric warming and solar activity. *Earth Planets and Space*, *66*(1). https://doi.org/10.1186/1880-5981-66-94

Laskar, F. I., Pallamraju, D., Lakshmi, T. V., Reddy, M. A., Pathan, B. M., & Chakrabarti, S. (2013). Investigations on vertical coupling of atmospheric regions using combined multiwavelength optical dayglow, magnetic, and radio measurements. *Journal of Geophysical Research: Space Physics*, *118*(7), 4618–4627. https://doi.org/10.1002/jgra.50426

Laskar, F. I., Pedatella, N. M., Codrescu, M. V., Eastes, R. W., Evans, J. S., Burns, A. G., & McClintock, W. (2021). Impact of GOLD retrieved thermospheric temperatures on a whole atmosphere data assimilation model. *Journal of Geophysical Research: Space Physics*, *126*(1). https://doi.org/10.1029/2020ja028646

Li, J., Wang, W., Lu, J., Yuan, T., Yue, J., Liu, X., et al. (2018). On the responses of mesosphere and lower thermosphere temperatures to geomagnetic storms at low and middle latitudes. *Geophysical Research Letters*, *45*(19), 10128–10137. https://doi.org/10.1029/2018GL078968

Liu, H., & Lühr, H. (2005). Strong disturbance of the upper thermospheric density due to magnetic storms: CHAMP observations. *Journal of Geophysical Research*, *110*(A9). https://doi.org/10.1029/2004ja010908

Liu, X., Yue, J., Wang, W., Xu, J., Zhang, Y., Li, J., et al. (2018). Responses of lower thermospheric temperature to the 2013 St. Patrick's Day geomagnetic storm. *Geophysical Research Letters*, *45*(10), 4656–4664. https://doi.org/10.1029/2018gl078039

Lumpe, J. D., Bevilacqua, R. M., Hoppel, K. W., & Randall, C. E. (2002). POAM III retrieval algorithm and error analysis. *Journal of Geophysical Research*, *107*(D21), 5–1. https://doi.org/10.1029/2002jd002137

Mandal, S., & Pallamraju, D. (2020). Thermospheric gravity wave characteristics in the daytime over low-latitudes during geomagnetic quiet and disturbed conditions. *Journal of Atmospheric and Solar-Terrestrial Physics*, *211*, 105470. https://doi.org/10.1016/j.jastp.2020.105470

Mayr, H. G., Harris, I., & Spencer, N. W. (1978). Some properties of upper atmosphere dynamics. *Reviews of Geophysics*, *16*(4), 539–565. https://doi.org/10.1029/rg016i004p00539

McClintock, W. E., Eastes, R. W., Beland, S., Bryant, K. B., Burns, A. G., Correira, J., et al. (2020). Global-scale observations of the limb and disk mission implementation: 2. Observations, data pipeline, and level 1 data products. *Journal of Geophysical Research: Space Physics*, *125*(5). https://doi.org/10.1029/2020ja027809

Mehta, P. M., Walker, A. C., Sutton, E. K., & Godinez, H. C. (2017). New density estimates derived using accelerometers on board the CHAMP and GRACE satellites. *Space Weather*, *15*(4), 558–576. https://doi.org/10.1002/2016sw001562

Meier, R. R., Picone, J. M., Drob, D., Bishop, J., Emmert, J. T., Lean, J. L., et al. (2015). Remote sensing of earth's limb by TIMED/GUVI: Retrieval of thermospheric composition and temperature. *Earth and Space Science*, *2*(1), 1–37. https://doi.org/10.1002/2014ea000035

Mikhailov, A. V., & Perrone, L. (2020). Poststorm thermospheric NO overcooling? *Journal of Geophysical Research: Space Physics*, *125*(1). https://doi.org/10.1029/2019ja027122

Pallamraju, D., Chakrabarti, S., & Valladares, C. E. (2004). Magnetic storm-induced enhancement in neutral composition at low latitudes as inferred by $O(^1D)$ dayglow measurements from Chile. *Annales Geophysicae*, *22*(9), 3241–3250. https://doi.org/10.5194/angeo-22-3241-2004

Pallamraju, D., Laskar, F. I., Singh, R. P., Baumgardner, J., & Chakrabarti, S. (2013). MISE: A multiwavelength imaging spectrograph using echelle grating for daytime optical aeronomy investigations. *Journal of Atmospheric and Solar-Terrestrial Physics*, *103*, 176–183. https://doi.org/10.1016/j.jastp.2012.12.003

Pant, T. K., & Sridharan, R. (1998). A case-study of the low-latitude thermosphere during geomagnetic storms and its new representation by improved MSIS model. *Annales Geophysicae*, *16*(11), 1513–1518. https://doi.org/10.1007/s00585-998-1513-8

Pant, T. K., & Sridharan, R. (2001). Seasonal dependence of the response of the low latitude thermosphere for external forcings. *Journal of Atmospheric and Solar-Terrestrial Physics*, *63*(10), 987–992. https://doi.org/10.1016/s1364-6826(01)00011-6

Prölss, G. W. (1980). Magnetic storm associated perturbations of the upper atmosphere: Recent results obtained by satellite-borne gas analyzers. *Reviews of Geophysics*, *18*(1), 183. https://doi.org/10.1029/rg018i001p00183

Rishbeth, H., & Garriott, O. K. (1969). *Introduction to ionospheric physics*. Academic Press.
Rodgers, C. D. (2000). *Inverse methods for atmospheric sounding*. World Scientific. https://doi.org/10.1142/3171
Spencer, N. W., Wharton, L. E., Niemann, H. B., Hedin, A. E., Carrignan, G. R., & Maurer, J. C. (1981). The dynamics explorer wind and temperature spectrometer. *Space Science Instrumentation*, *5*, 417–428.
Strickland, D. J., Cox, R. J., Meier, R. R., & Drob, D. P. (1999). Global o/n2derived from DE 1 FUV dayglow data: Technique and examples from two storm periods. *Journal of Geophysical Research*, *104*(A3), 4251–4266. https://doi.org/10.1029/98ja02817
Tsurutani, B. T., Verkhoglyadova, O. P., Mannucci, A. J., Saito, A., Araki, T., Yumoto, K., et al. (2008). Prompt penetration electric fields (PPEFs) and their ionospheric effects during the great magnetic storm of 30-31 October 2003. *Journal of Geophysical Research*, *113*(A5). https://doi.org/10.1029/2007ja012879
Zhang, Y., Paxton, L. J., & Schaefer, R. K. (2019). Deriving thermospheric temperature from observations by the global ultraviolet imager on the thermosphere ionosphere mesosphere energetics and dynamics satellite. *Journal of Geophysical Research: Space Physics*, *124*(7), 5848–5856. https://doi.org/10.1029/2018ja026379